J Mater Sci: Mater Electron **(2023) 34:2221**

Structural and optical characterization of beta-gallium oxide

Valentine W. Muramba[1,2,*], Abdulraoof I. A. Ali[1], and Jacqueline M. Nel[1]

[1] *Department of Physics, University of Pretoria, Private Bag X20, Hatfield, Republic of South Africa*
[2] *Department of Mathematics & Physics, Technical University of Mombasa, P.O. Box, Mombasa 90420-80100, Kenya*

Received: 15 September 2023
Accepted: 13 November 2023
Published online: 26 November 2023

ABSTRACT

Demands for cheaper solar cells have led researchers to less complex, low-temperature, vacuum-free thin-film deposition processes, like spray pyrolysis and sol–gel spin coating. Previous studies of β-Ga_2O_3 thin-film deposition have used aqueous solutions of gallium nitrate which have strong tendencies to form hydroxide precipitates. This leads to the blockage of spray gun nozzles. To avoid precipitation, tetrahydroxogallate (III) ammonium was used as a novelty precursor in this study for the synthesis of β-Ga_2O_3. In the spray pyrolysis technique, the precursor was deposited on sapphire substrates at 200 ℃, with a carrier gas pressure of 200 kPa. The same precursor, with added monoethanolamine to enhance viscosity, was used in the spin coating method. A polycrystalline β-Ga_2O_3 structure was obtained by post-annealing films at 750 ℃ in ambient air. The spin-coated films with thicknesses ranging from 165 to 354 nm exhibited an average crystallite size of 17.78 nm and an optical band gap range between 4.80 eV and 4.95 eV. Films produced by spray pyrolysis had thicknesses ranging between 158 and 255 nm, an average crystallite size of 17.55 nm, and a band gap ranging between 4.69 eV and 4.93 eV. From Raman spectroscopy, the molecular vibrational modes A_g and B_g were detected, featuring three blue shifts and two red shifts. Films showed a UV-blue region originating from oxygen and gallium vacancies in the lattice, an important characteristic for good photodetectors and vital for solar cell passivation. When utilizing β-Ga_2O_3 as dielectric coating, the refractive index between air and solar cells is reduced, enhancing solar energy absorption. Similar results were obtained for both synthesis techniques confirming the reliability of the methods.

1 Introduction

Energy crisis and environmental pollution are some of the main global challenges that hinder economic development. Renewable energy, including but not limited to solar, geothermal, and wind energy, as clean and abundant energy sources, is widely believed to be a promising way to address these challenges. Conversion of these energies into electricity and utilization is considered an effective way to address this global concern. Consequently, the research calling for materials that can enhance the conversion of renewable energy

Address correspondence to E-mail: valentinewabwire@gmail.com

https://doi.org/10.1007/s10854-023-11643-9

into electrical energy is a step in the right direction [1–3].

Semiconductor materials stand out uniquely in this research endeavor. Narrow band gap semiconductors like silicon find applications in producing solar energy cells although they are not yet very efficient. On the other hand, wide band gap semiconductors are particularly suitable in the wind and geothermal energy conversion to electricity and high-power optoelectronics, given their common characteristics of high breakdown voltage, high thermal stability, low-ON-state resistance, low leakage current, and to some extent, good thermal conductivity [4]. To achieve improved wide band gap semiconductors, other classes of semiconductors, including metal oxides, have also been investigated [5].

Wide band gap semiconductors (WBGS) are resorted to since they allow power electronic components to be smaller, faster, more reliable, and more efficient while still allowing devices to operate at much higher temperatures, voltage, and frequencies than those normally associated with semiconductors [6]. Until now, gallium nitride and silicon carbide of the WBGS have been studied extensively, but their physical properties have not met the application demands in high-power optoelectronic applications and excessive thermal energy experienced in geothermal and wind energy conversion to electricity. β-Ga_2O_3 has emerged to be the ideal WBGS for high-power optoelectronic applications and geothermal and wind energy conversion to electricity due to its physical properties, including high thermal resistance, high breakdown voltage, and low leakage current, among others [6]. They can also be applied in dielectric coatings of solar cells and their passivation to minimize reflection and corrosion thereby increasing their stability and hence lifespan [2, 7–11].

The synthesis method and starting precursors in the production of thin films affect the properties of the final thin-film materials [7, 12]. Previously employed processes in the production of β-Ga_2O_3 like chemical vapour deposition and halide vapour epitaxy required a vacuum and fume chamber as the process involved hazardous fumes [13]. Some like metal–organic chemical vapour deposition and chemical dip coating require more than one oxidizing agent like water, oxygen, and nitrous oxide making the process complex. Thermal vapour deposition relies heavily relied on a vacuum for the process to be successful [16]. Therefore, the synthesis of β-Ga_2O_3 by spray pyrolysis and sol–gel spin coating methods will remedy some of the disadvantages mentioned as these techniques are vacuum-free solution-based processes.

Previous studies synthesized β-Ga_2O_3 by hydrous dissolving gallium nitrate in water. This solution had a strong tendency to form gallium hydroxide. The gallium hydroxide tended to precipitate and therefore caused blockage of spray gun nozzles. This could only be avoided by creating an acidic solution of stabilizing Ga^{3+} ions by acetylacetonate which has low solubility in an aqueous solution [14]. To avoid precipitation of the start-up precursor and the cumbersome process, tetrahydroxogallate (III) ammonium was used as a novelty precursor in this study for the synthesis of β-Ga_2O_3.

Depending on the growth conditions and crystal structure, Ga_2O_3 can function as either an insulator or an n-type wide band gap semiconductor [13]. This research explored the viability of spray pyrolysis and spin coating techniques as potential synthesis methods for β-Ga_2O_3. We compared the structural and optical properties of the thin films produced using these synthesis techniques and consequently established the optimal concentration of gallium nitrate in the precursor based on the optical and structural property values obtained to be a benchmark for future research. This optimization of precursor concentration is another novelty of this research.

2 Methodology

2.1 Sample preparation

The β-Ga_2O_3 was prepared by dissolving hydrated gallium nitrate salt (Merck) in 20 ml of 32% concentrated ammonium hydroxide (Merck) to produce the precursor tetrahydroxogallate (III) ammonium which has a high pH of 11.93 [15]. The prepared precursor had varying concentrations of 0.02 M, 0.03 M, 0.04 M, 0.05 M, and 0.06 M of hydrous gallium nitrate in tetrahydroxogallate (III) ammonium of which by mole concept translated to 5.0 at%, 7.5 at%, 10.0 at%, 12.5 at%, and 15.0 at% of gallium nitrate in the precursor (herein referred to as precursor concentration). The precursor solution was stirred using a magnetic stirrer at 25 ℃ and 150 rpm for 1.5 h to achieve a homogeneous solution. To ensure complete dissolution, the precursor was kept at room temperature for 24 h and was then directly used for spray pyrolysis. For sol–gel

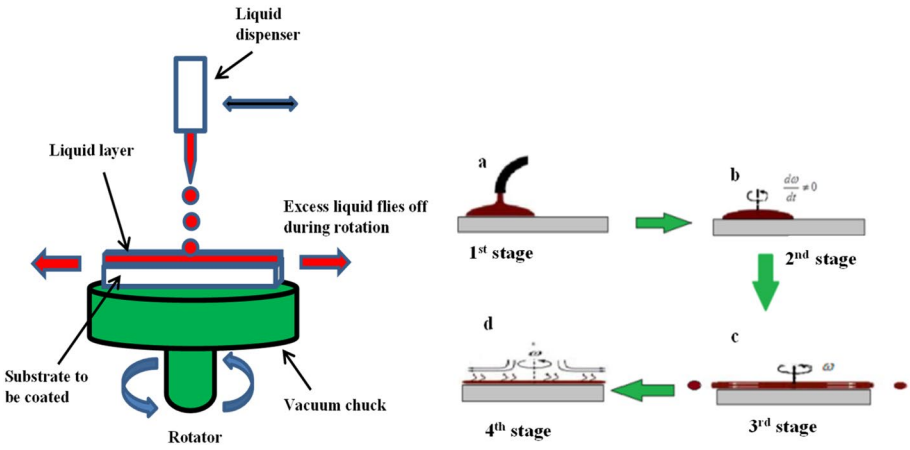

Fig. 1 Spin coating steps: **a** solution deposition, **b** spinner acceleration, **c** continuous solution spreading at constant angular speed, and **d** solution evaporation and film thinning [15]

spin coating, the precursor's viscosity was increased by adding monoethanolamine (C_2H_7NO) and left for 24 h to allow the formation of colloids [16].

The heterogeneous reaction involved in the production of β-Ga_2O_3 originated from the reaction of hydrated gallium nitrate with concentrated ammonium hydroxide, resulting in the formation of tetrahydroxogallate (III) ammonium and ammonium nitrate. The decomposition of this compound produced beta-phase gallium oxide and nitrogen gas [15].

The tetrahydroxogallate (III) ammonium does not form precipitates that could otherwise lead to nozzle clogging and inhomogeneous film deposition during spray pyrolysis [15]. The samples deposited on the sapphire substrate using spray pyrolysis and sol–gel spin coating were optically and structurally characterized, and the results were compared.

2.1.1 Spin coating deposition

The spin coating deposition was carried out on flat 1-cm^2 sapphire substrates, and the process was divided into four stages: deposition, spin-up, spin-off, and evaporation, as illustrated in Fig. 1. The precursor solution was dropped in the center of the stationary substrate. It was subsequently accelerated at an angular acceleration of 3.598 rad/s^2 to a spinning revolution of 3000 rpm for 30 s [15]. The samples were then dried in the oven at 40 ℃ for four minutes before applying an additional layer at room temperature. The process was repeated five times to achieve a good film. Post-annealing was conducted at 750 ℃ in ambient air for 15 min to obtain the desired β-Ga_2O_3.

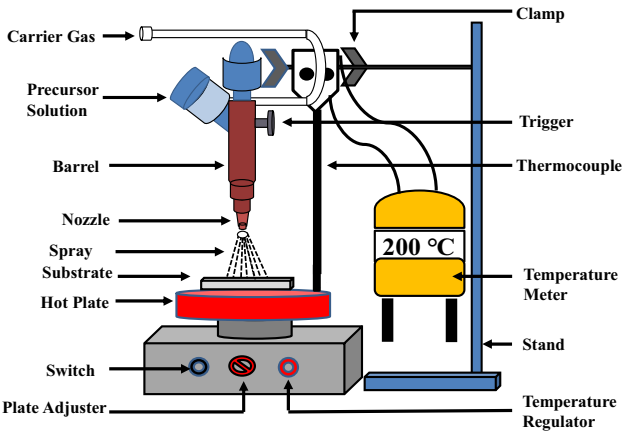

Fig. 2 Schematic diagram of the spray pyrolysis setup

2.1.2 Spray pyrolysis deposition

The spray pyrolysis technique is typically used to deposit the materials in thin-film form. The deposition setup consisted of a spray gun connected to the nitrogen carrier gas line, a hot plate, and a thermocouple. The schematic view of this setup is shown in Fig. 2.

The β-Ga_2O_3 was deposited pyrolytically onto a 1-cm^2 sapphire substrate. The precursor solution of tetrahydroxogallate (III) ammonium and the nitrogen carrier gas were passed through the spray nozzle at 0.035 L per minute deposition rate. To maintain an average hot plate temperature of 200 °C, spraying was carried out in two bursts per second with a three-second interval between each successive set of two bursts [16, 17]. In total, fourteen bursts were used for all depositions, while the carrier gas pressure was maintained at 200 kPa.

Post-annealing was then conducted at 750 ℃ in ambient air for 15 min to obtain the desired β-Ga_2O_3.

2.2 Sample characterization

2.2.1 Structural characterization

The imaging of the microstructure and morphology of films were determined using a Scanning Electron Microscope (FEGSEM: Zeiss 540 Ultra) operating at 2.0 kV. Energy-Dispersive X-ray Spectroscopy (FEGSEM: Zeiss 540 Xbeam) was utilized to identify the element composition of samples, percentage weight of elements, and stoichiometry of synthesized films, making it possible to identify dominant elements. X-ray diffraction was employed to investigate the crystal structure by determining the orientation and crystallite size of the material. This was carried out using a Bruker D2 Phaser X-ray diffractometer (XRD) with CuK_α radiation, a 1.5406 Å source, and scanning speed of 0.05° per second for 2θ at 15°–60° range.

From the XRD spectrum, the average crystallite size (D) is calculated using Williamson–Hall's formula of equation:

$$\beta\cos\theta = \frac{k\lambda}{D} + 4\varepsilon\sin\theta, \tag{1}$$

where β is the full-width-at-half-maximum (FWHM) of the diffraction peak intensity at the diffraction angle 2θ, k is the Scherrer constant ($k = 0.9$), λ is the wavelength $\lambda = 1.5406$ Å, and ε is the strain. For spray pyrolysis films, the peak position (2θ) at 21.09° (− 201 orientation) and 27.78° (400 orientation) were used, whereas for spin-coated films, 20.97° (− 201 0rientation) and 27.78° (400 orientation) were used.

The plot of cos θ against sin θ gave the slope (4ε) and the intercept ($k\lambda/D$) from which strain and crystallite size were calculated, respectively. Lattice parameters a, b, c, and γ were calculated from the same orientations, (− 201) and (400), to confirm the monoclinic structure of β-Ga_2O_3.

For the Raman spectroscopy, a WITec alpha 300 RAS + confocal Raman microscope with 532-nm excitation was employed. This technique was used to identify the vibrational modes of the molecules when compared to calculated local density approximation (LDA) and previous experimental data of the β-Ga_2O_3 functional groups.

2.2.2 Optical characterization

Film thickness (d) was measured using a Tencor Alpha Step 2000 Profilometer. Transmittance and absorbance measurements were conducted at near normal incidence in the wavelength range from 200 to 800 nm using Cary 100 Bio UV–vis spectroscopy. The absorption coefficient (α) is subsequently determined using Beer–Lambert's formula (2):

$$\alpha = 2.303\frac{A}{d}, \tag{2}$$

where A represents the optical absorbance obtained as the peak absorbance value of the spectra and 2.303 is the conversion factor from a decimal to a natural logarithm [16]. Similar results were obtained from transmittance spectra (3):

$$\alpha = \frac{1}{d}\left(-\log_{10}\frac{\%T}{100}\right), \tag{3}$$

where T is the peak transmittance value of the obtained spectra [18].

The relation between the absorption coefficient (α) and the photon energy ($h\nu$) is described in Eq. (4):

$$(\alpha h\nu)^{\frac{1}{n}} = A\left(h\nu - E_g\right). \tag{4}$$

This equation was used to determine the optical band gap (E_g), where A is a constant and n depends on the type of transition. In this case, a direct transition occurs, so $n = ½$ [19].

From Eq. (4), the absorption coefficient varies as $\left(h\nu - E_g\right)^{\frac{1}{2}}$. Plots of $(\alpha h\nu)^2$ versus photon energy ($h\nu$) in the high absorption region with extrapolations of the curves to ($h\nu$) axis at $(\alpha h\nu)^2 = 0$ gave direct energy band gap, E_g [19].

3 Results and analysis

3.1 Structural analysis

This included SEM imaging structure and morphology, EDX elemental composition and percentage, XRD plane orientations and crystallite size, and Raman molecular vibrational modes of various sprayed and spin-coated films.

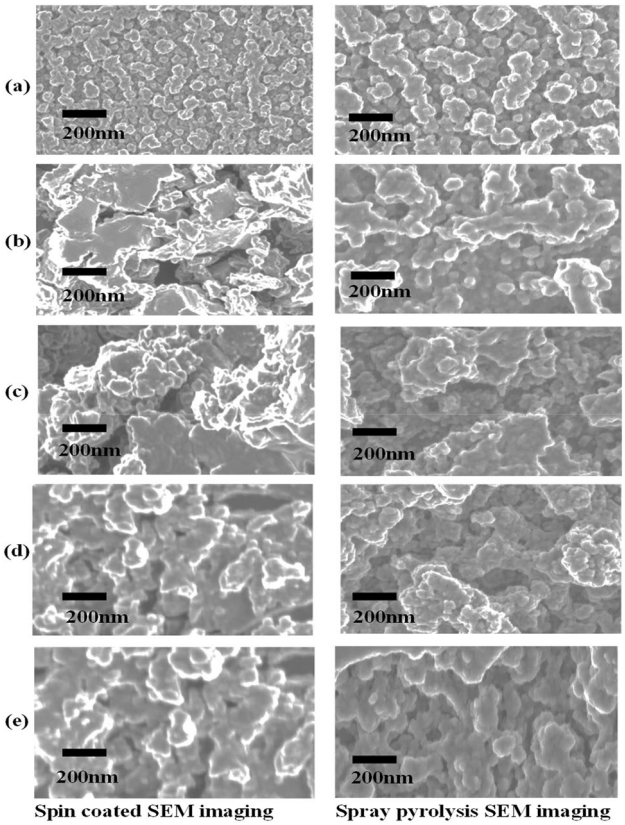

Fig. 3 SEM of spin-coated and pyrolytically sprayed thin films of β-Ga_2O_3 at varied concentrations **a** 5.0 at%, **b** 7.5 at%, **c** 10.0 at%, **d** 12.5 at%, and **e** 15.0 at%, after post-annealing at 750 °C

concentrations, but with similar surface features for the same concentration. EDX spectroscopy confirmed that gallium and oxygen dominated the samples with some aluminum, likely originating from the sapphire substrate. This trend was similar for films obtained from both spin coating and spray pyrolysis.

The morphology of the initial 5.0-at% spin-coated film has smaller agglomerates compared to the sprayed films of the same concentrations, where the agglomerates were larger. In subsequent films with higher concentrations, the morphologies were not significantly different. At concentrations of 7.5 at% and higher, the agglomerates are larger than those observed in 5.0 at%, but there is not a significant change in the morphology for the higher concentrations.

3.1.2 *Orientation, lattice parameters, and vibrational modes*

XRD analysis was used to determine the orientation and crystallite size of the material. The diffractograms exhibited the monoclinic structure of β-Ga_2O_3. The peak intensity of gallium oxide deposited by spray pyrolysis was higher compared to the spin-coated films, but the orientations of planes were consistent, as demonstrated in Fig. 4 at (− 201) and (400).

The XRD patterns of both the sprayed and spin-coated films displayed a shift to lower angles relative

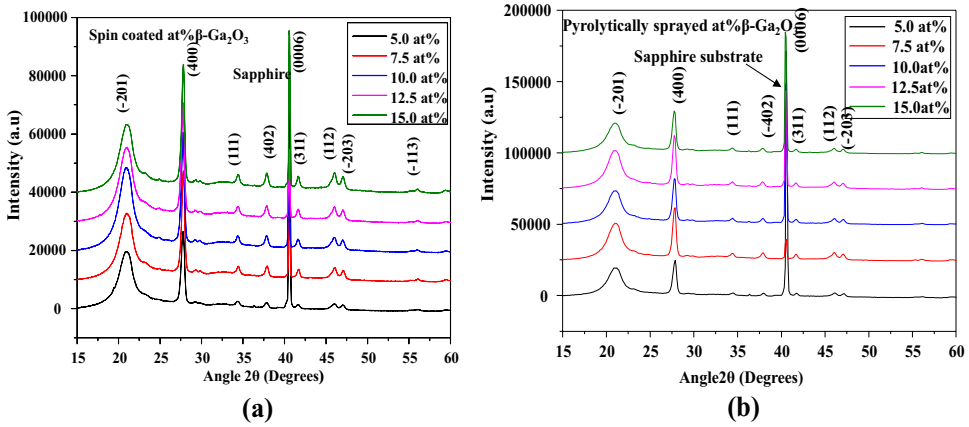

Fig. 4 X-rays diffractograms of **a** spin-coated and **b** pyrolytically sprayed β-Ga_2O_3 deposited on sapphire and post-annealed at 750 °C in ambient air

3.1.1 *Morphology and elemental analyses*

The SEM image in Fig. 3 revealed porous structures in both spin-coated and pyrolytically sprayed thin films, displaying different grain sizes for various

to the theoretical JCPDS data (No. 11–370). In this study, the (400) peak (at angle $2\theta = 28°$) had the highest intensity, whereas, in JCPDS data (No. 11–370), the (-202) peak (at angle $2\theta = 32°$) had the highest intensity. However, both experimental and theoretical

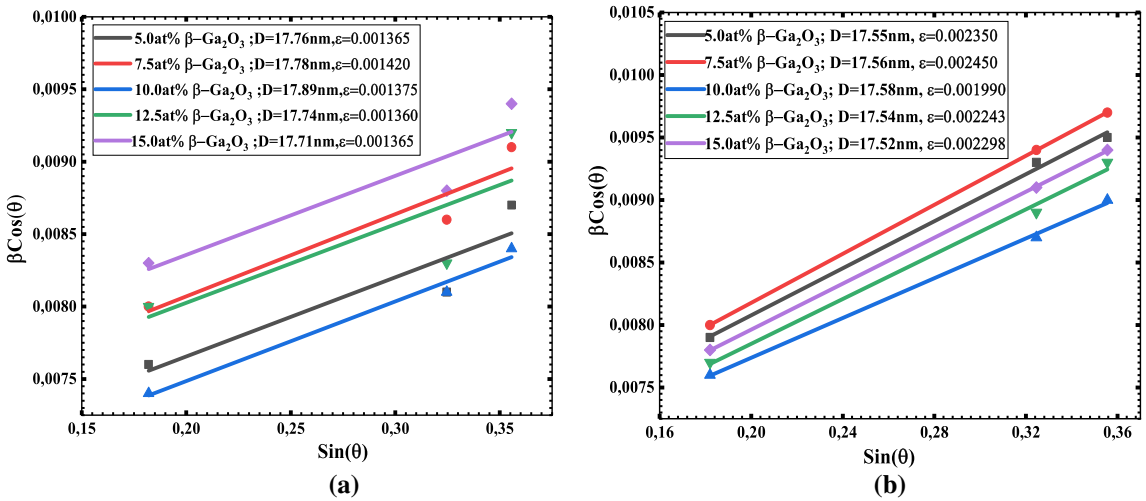

Fig. 5 Plots of the Williamson–Hall formula for **a** spin-coated and **b** pyrolytically sprayed β-Ga_2O_3 films from which crystallite size (D) and the strain (ε) were determined

Table 1 Calculated average structural parameters of β-Ga_2O_3 and previous theoretical/experimental results

β-Ga_2O_3	a (nm)	b (nm)	c (nm)	γ (°)
Spin coated	1.249	0.310	0.590	103.71
Pyrolytically sprayed	1.221	0.304	0.580	103.82
Experimental Ref [17]	1.234	0.308	0.587	103.90
Theoretical Ref [18]	1.255	0.308	0.589	103.67
Previous experiment [18]	1.222 ± 0.002	0.304 ± 0.001	0.580 ± 0.001	103.70

values exhibited a (400) peak to have a higher intensity than the (-201) peak. The absence of a (-202) peak from the XRD patterns indicates that there is some preferred orientation in the films.

The FWHM (β) obtained from the (-201) and (400) peaks were used to calculate the average crystallite sizes (D) using the Williamson–Hall formula of Eq. (1). For spin-coated and pyrolytically sprayed samples, the calculated average crystallite sizes were 17.7748 ± 0.5 nm and 17.5487 ± 0.5 nm, respectively. The strain of the films was also determined by applying Eq. (1) to Fig. 5, yielding average strain values of 1.377×10^{-3} and 2.266×10^{-3} for spin-coated and pyrolytically sprayed samples, respectively.

The difference in the strain can be attributed to the temperature of the substrates at the time of film deposition. Since the pyrolytically sprayed samples were prepared at higher substrate temperatures (200 ℃) compared to spin-coated films (prepared at room temperature, i.e., 28 ℃) for the same precursor concentration, this could have contributed to higher strains in pyrolytically sprayed films.

From Fig. 5, the nonlinear points were an indication of non-uniform film distribution in spin coating techniques compared to pyrolytically sprayed films. It was also noticed that the 10-at% precursor concentration exhibited the largest crystallite size and lowest strain. Away from this concentration, the films demonstrated smaller crystallite size and higher strain. This can be attributed to the fact that lower precursor concentrations of 5.0 at% and 7.5 at% had less particle layer overlap compared to 10.0-at% films. But as the particle layers build up as in 12.5 at% and 15.0 at%, high nuclear-electron attraction increases which causes particles to reduce in their atomic radii and increase strain in the structure. This led to optimal concentration for crystallite size and strain of films at 10.0 at%.

Further, the lattice parameters for β-Ga_2O_3 films were determined and are shown in Table 1. These were compared to values for films reported by others [17, 18]. The results were consistent with the theoretical and experimental results, confirming the monoclinic β-Ga_2O_3.

The Raman spectroscopy was employed to complement XRD analysis in characterizing β−Ga_2O_3 [20].

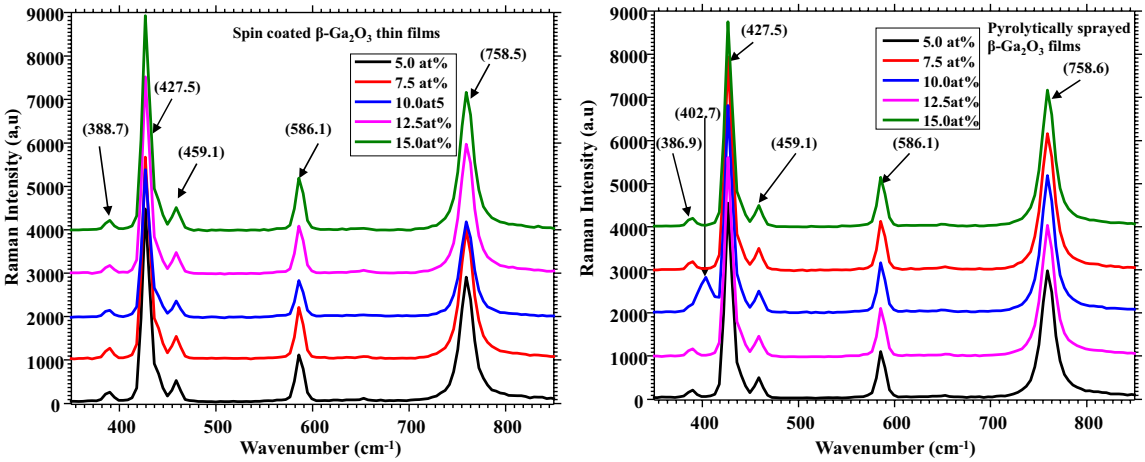

Fig. 6 Raman spectra of spin-coated and pyrolytically sprayed β-Ga_2O_3 post-annealed at 750 °C

Table 2 LDA calculated and experimental functional groups data vibrational modes of β-Ga_2O_3 on sapphire substrate

Sample No	1	2	3	4	5	6	7	8	9	10	11	12	13	14	15
Mode Symmetry	A_g	B_g	B_g	A_g	A_g	A_g	A_g	B_g	A_g	A_g	B_g	A_g	B_g	A_g	A_g
LDA calculated wavenumber (cm^{-1}) [20, 21]	104	113	150	160	207	317	348	356	414	469	474	601	624	635	732
Experimental data wavenumber (cm^{-1}) [20, 21]	111	114	147	169	199	318	346	353	415	475	–	628	651	657	763
This Work wavenumber (cm^{-1})	–	–	–	–	–	–	387	402	428	459	586	–	–	–	758
Wavenumber shift (cm^{-1})	–	–	–	–	–	–	+41	+49	+13	−16	–	–	–	–	− 5

The Raman spectra for both spin-coated and pyrolytically sprayed samples are presented in Fig. 6.

The Raman peaks in the spin-coated films appeared at the same wavenumber positions as those in spray pyrolysis, but the intensity was higher for the spin-coated samples. Five vibrational modes of β-Ga_2O_3 were identified as A_g and B_g at wavenumbers 386.9 cm^{-1}, 427.5 cm^{-1}, 459.1 cm^{-1}, 586.1 cm^{-1}, and 758.6 cm^{-1}. Additionally, the spray pyrolysis sample with the 10.0-at% solution concentration exhibited the sixth vibrational mode at wavenumber 402.7 cm^{-1}. These findings were consistent with previously calculated LDA data and experimental data on β-Ga_2O_3 functional groups [21, 22]. The peaks that were not consistent with the LDA data such as one at wavenumber 586.1 cm^{-1} (Table 2) were identified to be associated with bending and stretching modes in the sapphire substrate and defects in samples.

The peaks at wavenumbers 386.9 cm^{-1}, 402.7 cm^{-1}, and 427.5 cm^{-1} exhibited a blue shift, whereas 459.1 cm^{-1} and 758.6 cm^{-1} exhibited a red shift compared to the LDA functional group data. The peak 586.1 cm^{-1} showed no shift with respect to experimental data of LDA functional group data. A significant number of defects have been linked to the red shift, while blue shifts were observed in other cases [22].

These results provided evidence that the samples under investigation consisted of β-Ga_2O_3 in agreement with functional group data of previous studies. Furthermore, the samples were found to be stable under the X-ray beam and green laser used in Raman spectroscopy during our investigation.

3.2 Optical analysis

UV–vis spectroscopy was used to analyze transmittance and absorbance spectra in the wavelength range of 200 nm–800 nm. The graphs in Figs. 7 and 8 were analyzed alongside the film thicknesses that were measured using a profilometer.

From Fig. 7, when considering the absorbance at a wavelength of 600 nm, absorbance values for samples synthesized by spin coating ranged between 4.5% (or 0.045) and 13.0% (or 0.13), whereas those pyrolytically sprayed films ranged between 0.6% (or 0.006) and 4.2% (or 0.042). The samples prepared by spray pyrolysis demonstrated lower absorbance compared

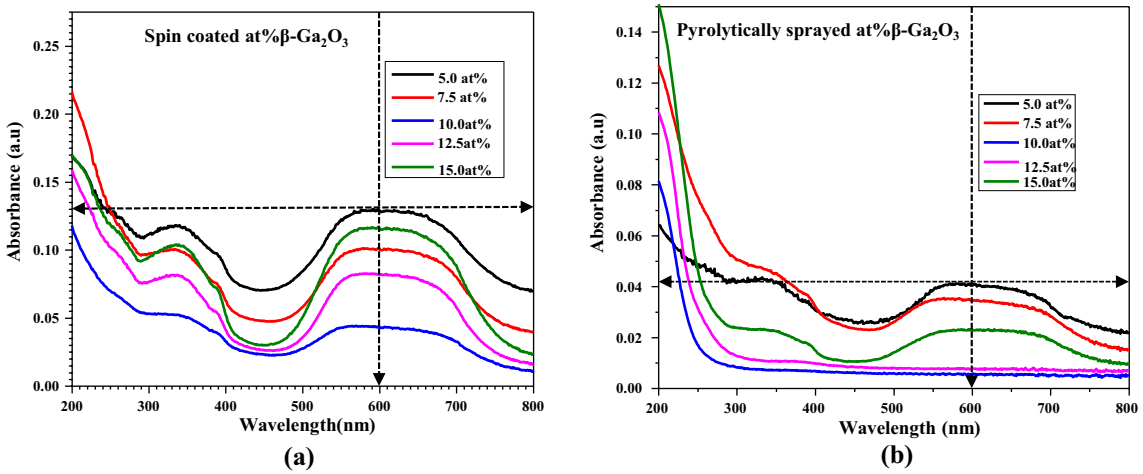

Fig. 7 Absorbance spectra of β-Ga_2O_3 deposited by **(a)** spin coating and **b** spray pyrolysis at various concentrations

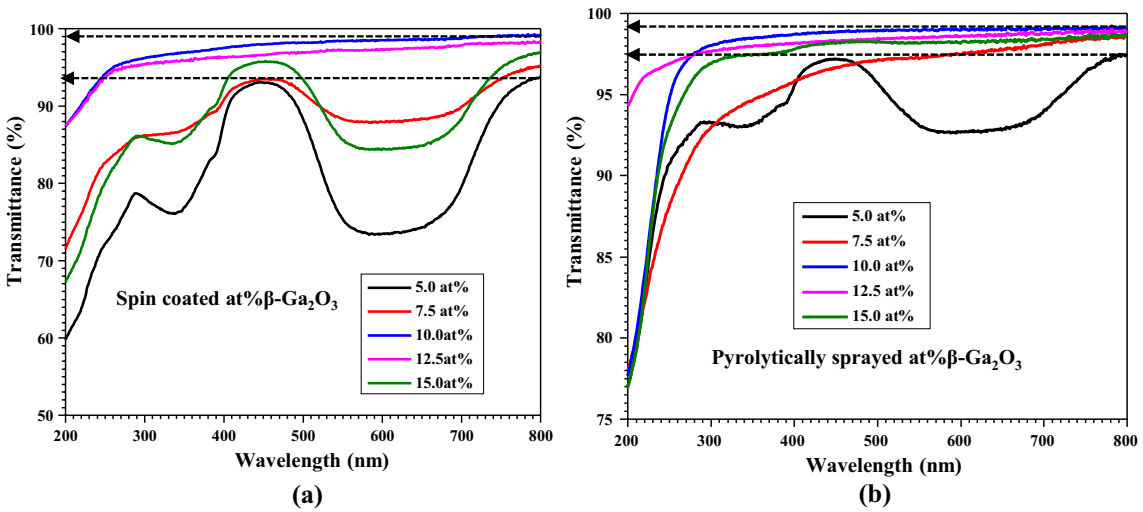

Fig. 8 Transmittance spectra for the various concentrations of β-Ga_2O_3 deposited by **a** spin coating and **b** spray pyrolysis

to spin-coated samples, as depicted in Fig. 7. The same trend was observed in the transmittance spectra, as depicted in Fig. 8 for both spin-coated and pyrolytically sprayed samples.

In the wavelength range of 600 nm–800 nm, the spin-coated materials exhibited transmittance levels between 93% and 98.5%, whereas sprayed samples transmitted light in the range of 97% and 99%, as shown in Fig. 8. In both cases, it can be noted that the sample with 10 at % concentration demonstrated the lowest absorbance and highest transmittance. From Figs. 7 and 8, at UV–vis wavelength range of 600 nm–800 nm, the high transmittance and low absorbance is an indication that the particles in the β-Ga_2O_3 had very few bonds with vibrational energy that corresponded to the frequency of incident light at the point of matter–light interaction. High absorbance by spin-coated films compared to pyrolytically sprayed of the same precursor concentration is attributed to non-uniform film distribution in the former caused by the acceleration of substrate during spinning and defects in crystals that absorb certain frequencies.

Film thicknesses were measured using profilometry. These values were used to calculate absorption coefficients from Beer–Lambert's formula from Eq. (2). These two parameters were then used in

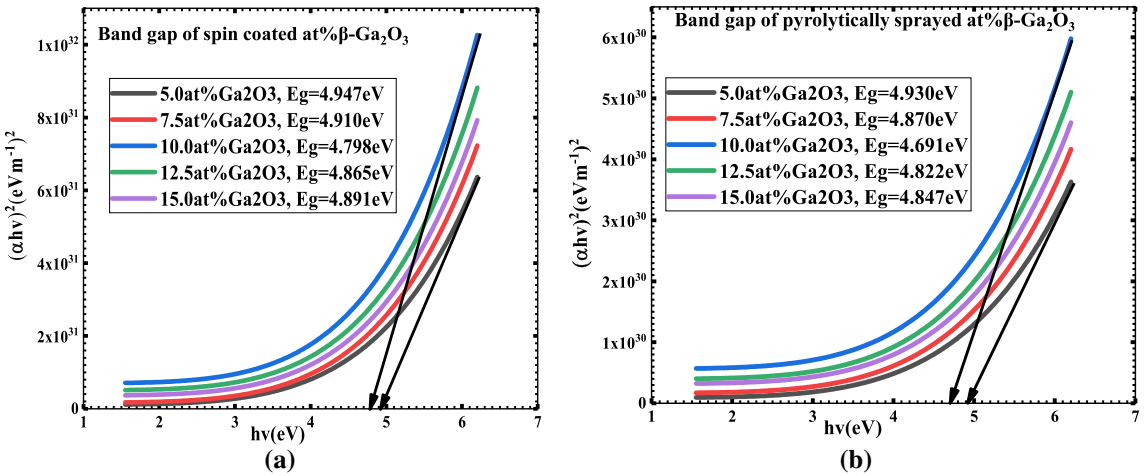

Fig. 9 Tauc plots used to determine the optical band gaps of β-Ga_2O_3 deposited by **a** spin coating and **b** spray pyrolysis

Table 3 Spin-coated films absorbance at 600 nm, average layer thickness, and energy band gap

at% β-Ga_2O_3	Absorbance *A* (a.u)	Thickness *d* (nm)	Band gap *Eg* (eV)
5.0 at%	0.130	164.99	4.95
7.5 at%	0.103	167.24	4.91
10.0 at%	0.045	281.13	4.80
12.5 at%	0.085	298.31	4.87
15.0 at%	0.118	354.12	4.89

Table 4 Spray pyrolysis films absorbance at 600 nm, average layer thickness, and energy band gap

at% β-Ga_2O_3	Absorbance *A* (a.u)	Thickness *d* (nm)	Band gap *Eg* (eV)
5.0 at%	0.042	158.21	4.93
7.5 at%	0.037	170.35	4.87
10.0 at%	0.006	200.29	4.69
12.5 at%	0.008	231.67	4.82
15.0 at%	0.023	255.20	4.85

Eq. (4) to plot the graphs shown in Fig. 9, from which the optical energy band gaps were determined.

The results obtained are tabulated in Tables 3 and 4 indicating optical energy band gaps ranging from 4.69 eV to 4.95 eV. These results agreed with the literature results [23], which fall within the range of 4.66 eV to 4.99 eV.

4 Summary of results

The summary of the samples' properties was compared for spin-coated and pyrolytically sprayed samples, as shown in Tables 5 and 6, respectively. The XRD peak ratios of peak (400)-to-peak (- 201) and Raman spectra peak ratios at wavenumbers 428 cm^{-1} to 759 cm^{-1} were also determined.

The higher XRD and Raman spectra peak ratios observed in spin-coated films compared to pyrolytically sprayed films indicate a greater degree of particle alignment along (400) direction, suggesting a more uniform structure in pyrolytically sprayed films than spin-coated films. The spin-coated films have a wider FWHM, β, for the (400) peak, implying a larger crystallite size in comparison to the pyrolytically sprayed films. The determined optical band gaps fell within the range of the previous studies, ranging from 4.66 eV to 4.96 eV. The synthesized films exhibited molecular vibrational modes of β-Ga_2O_3, namely A_g and B_g, as confirmed by Raman spectroscopy. Overall, the structural and optical properties of samples synthesized by spin coating closely resembled those synthesized by spray pyrolysis.

Table 5 Summary of properties of spin-coated thin films

Precursor (at% Con.)	XRD peak ratio (400): (− 201)	FWHM (400) β (Rad)	Crystallite size D (nm)	Raman Spectra Peak Ratio at wavenumbers 428 cm^{-1} and 759 cm^{-1}	Film thickness d (nm)	Transmittance at $\lambda > 780$ nm (%)	Absorbance at $\lambda = 600$ nm (%)	Optical band gap Eg (eV)
5.0	1.32	0.0084	17.7571	1.54	164.99	87.02	13.0	4.95
7.5	1.58	0.0083	17.7753	1.54	167.24	89.24	10.3	4.91
10.0	1.41	0.0085	17.8868	1.52	281.13	96.09	4.50	4.80
12.5	1.56	0.0081	17.7424	1.51	298.31	90.70	8.50	4.87
15.0	1.82	0.0084	17.7123	1.54	354.12	87.59	11.8	4.89

Table 6 Summary of properties of pyrolytically sprayed thin films

Precursor (at% Con.)	XRD peak ratio (400):(− 201)	FWHM (400) β (Rad)	Crystallite size D (nm)	Raman Spectra Peak Ratio at wavenumbers 428 cm^{-1} and 759 cm^{-1}	Film thickness d (nm)	Transmittance at $\lambda > 780$ nm (%)	Absorbance at $\lambda = 600$ nm (%)	Optical band gap Eg (eV)
5.0	1.24	0.0078	17.5518	1.53	158.21	94.62	4.20	4.93
7.5	1.39	0.0081	17.5623	1.55	170.35	95.73	3.70	4.87
10.0	1.33	0.0083	17.5792	1.51	200.29	98.44	0.60	4.69
12.5	1.36	0.0084	17.5347	1.40	231.67	96.78	0.80	4.82
15.0	1.37	0.0079	17.5154	1.49	255.20	96.35	2.30	4.85

5 Conclusion

β-Ga_2O_3 thin films were successfully synthesized from tetrahydroxogallate (III) ammonium by sol–gel spin coating and spray pyrolysis techniques. The results and analysis in this study demonstrated that the structure and morphological characteristics analyzed by EDS, SEM, XRD, and Raman spectroscopy confirmed the formation of β-Ga_2O_3 with crystalline structures obtained after annealing at 750 ℃ in air.

An important contribution of this research is the identification of tetrahydroxogallate (III) ammonium as a novel starting precursor solution for synthesizing β-Ga_2O_3 through uncomplicated, cost-effective, and vacuum-free synthesis techniques; namely, spray pyrolysis and sol–gel spin coating. These methodologies have not been previously explored for this purpose.

The 10 at% concentration of gallium nitrate in ammonium hydroxide produced the best result in both spray pyrolysis and spin coating compared to prior studies previously mentioned concerning β-Ga_2O_3. This study has shown that 10 at% of tetrahydroxogallate (III) ammonium is the optimal precursor concentration. These results form the basis for further structural and optical investigations of β-Ga_2O_3. To the author's knowledge, this optimization has not been done before and neither has tetrahydroxogallate (III) ammonium been applied as a precursor in the synthesis of β-Ga_2O_3 by any synthesis technique.

Acknowledgements

The authors would like to thank. The Technical University of Mombasa for the opportunity and financial support during this study and The University of Pretoria and the South African National Research Foundation (NRF) for financial support during this study under Grant Numbers 111744 and 137,977.

Author contributions

All authors contributed to the study's conception and design. Material preparation, data collection, and analysis were performed by all authors. The first draft of the manuscript was written by Valentine Muramba, and all authors commented on previous versions of manuscripts. All authors read and approved the final manuscript.

Funding

Open access funding provided by University of Pretoria. This work was financially supported by the South African National Research Foundation (NRF) during this study under Grant Numbers 111744 and 137977.

Data availability

The author declares that the data supporting the findings of this study are available within the paper. Any secondary data the author has reused, repository DOI is cited in the reference. Any raw data generated during this study are available from the corresponding author on reasonable request.

Declarations

Competing interests The authors declare they have no relevant financial or non-financial interests to disclose.

References

1. Z. Hu, K. Nomoto, W. Li, N. Tanen, K. Sasaki, A. Kuramata, T. Nakamura, D. Jena, H.G. Xing, IEEE Electron Device Lett (2018). https://doi.org/10.1109/LED.2018.2830184
2. M.H. Wong, Y. Nakata, A. Kuramata, S. Yamakoshi, M. Higashiwaki, Appl. Phys. Express (2017). https://doi.org/10.7567/APEX.10.041101
3. H. Zhou, M. Si, S. Alghamdi, G. Qiu, L. Yang, P.D. Ye, IEEE Electron. Device. Lett. (2017). https://doi.org/10.1109/LED.2016.2635579
4. Y. Jae-Hyuck, R. Subrina, L. Andrew, Z. Hongping, E. Selim, Appl. Mater. (2018). https://doi.org/10.1063/1.5021603
5. M. Kim, J.-H. Seo, U. Singisetti, Z. Ma, J. Mater. Chem. (2017). https://doi.org/10.1039/c7tc02221b
6. S.J. Pearton, Y. Jiancheng, H.C. Patrick, F. Ren, K. Jihyun, J.T. Marko, A.M. Michael, Appl. Phys. Rev. (2018). https://doi.org/10.1063/1.5006941.
7. D. Huiyang, J.L. Kenneth, M. Yu, S.B. Dylan, E.U. Karel, M. Joshua, K. Martin, C. Andrew, H. Peter, S. Olav, L.B. Robert, S.H. James, Adv. Opt. Mater. (2020). https://doi.org/10.1002/adom.201901522.
8. C. Xuanhu, R. Fangfang, G. Shulin, Y. Jiandong, Photonics Res. (2019). https://doi.org/10.1364/PRJ.7.000381
9. D. Li, K. Jiang, X. Sun, C. Guo, Adv. Apt. Photonics (2018). https://doi.org/10.1364/AOP.10.000043
10. K. Sasaki, A. Kuramata, T. Masui, E.G. Víllora, K. Shimamura, S. Yamakoshi, Appl. Phys. Express (2012). https://doi.org/10.1143/APEX.5.035502
11. K. Sasaki, M. Higashiwaki, A. Kuramata, T. Masui, S. Yamakoshi, Appl. Phys. Express. (2013). https://doi.org/10.7567/APEX.6.086502;
12. H.S. Mohamed, M.G. Mohammed, W.H. Eisa, M. Boshta, Emergent. Mater (2023). https://doi.org/10.1007/S42247-023-00557-1
13. Han S.-H, Mauze A, Ahmadi E, Mates T, Oshima Y, Speck J.S (2018) AIP Adv. https://doi.org/10.1063/5.0044923
14. Nina W, Rachmat A.W, Wolfgang K, Giovani L, Emil J.W.L, Theodoros D (2019) J Mater Chem C https://doi.org/10.1039/C8TC04157A
15. B.C. Lay, A.M.O. Rozana, P. Poopalan, AIP Conf. (2020). https://doi.org/10.1063/1.5142120
16. H.Y. Playford, A.C. Hannon, E.R. Barney, R.I. Walton, Chem. A. Eur. J. (2013). https://doi.org/10.1002/chem.201203359.
17. Y. Kokubun, K. Miura, F. Endo, S. Nakagomi, Appl. Phys. Lett. (2007). https://doi.org/10.1063/1.2432946

18. S. Constance, F. Axcel, R.T.Z. Dietrich, Phys. Stat. Sol. (2016). https://doi.org/10.1002/pssa.200778856
19. Jung J. -Y, Cho W. -S, Kim J. -H, Hwang K. -T, Kang E. -T, Han K. –S (2016) Ceram Int DOI: https://doi.org/10.1016/j.ceramint.2015.10.061
20. M. Valentine, M. Maxwell, G. Francis, O. Victor, M. Robinson, M. Silas, A. Kennedy, Am. J. Mater. Sci. (2015). https://doi.org/10.5923/j.materials.20150502.01
21. S. Kumar, G. Sarau, C. Tessarek, M.Y. Bashouti, A. Hähnel, S. Christiansen, R. Singh, Phys. D: Appl. Phys. (2014). https://doi.org/10.1088/0022-3727/47/43/435101
22. Rao R (2007) Clemson University, Tiger Prints; Condensed Matter Physics Commons. All Dissertations. 73. https://tigerprints.clemson.edu/all_dissertations/73
23. C. Yang, H. Liang, Z. Zhang, X. Xia, P. Tao, Y. Chen, H. Zhang, R. Shen, Y. Luo, G. Du, RSV Adv. (2018). https://doi.org/10.1039/C8RA00523K